IEEE Access
Multidisciplinary | Rapid Review | Open Access Journal

Received May 17, 2017, accepted June 19, 2017, date of publication June 27, 2017, date of current version August 22, 2017.

Digital Object Identifier 10.1109/ACCESS.2017.2720591

A Novel Dual-Broadband Dual-Polarized Electrical Downtilt Base Station Antenna for 2G/3G Applications

YEJUN HE, (Senior Member, IEEE), WEI TIAN, AND LONG ZHANG

Shenzhen Key Laboratory of Antennas and Propagation, Guangdong Engineering Research Center of Base Station Antennas and Propagation, College of Information Engineering, Shenzhen University, Shenzhen 518060, China

Corresponding author: Yejun He (heyejun@126.com)

This work was supported in part by the National Natural Science Foundation of China under Grant 61372077, in part by the Science and Technology Innovation Commission of Shenzhen under Grant ZDSYS 201507031550105, and in part by Guangdong Provincial Science and Technology Programs under Grant 2013B090200011 and Grant 2016B090918080.

ABSTRACT A novel dual-broadband dual-polarized base station antenna array with compact structure and low profile is proposed in this paper for the existing mobile communication system operating over 0.79–0.96 GHz (European Digital Dividend/CDMA/GSM) and 1.71–2.17 GHz (DCS/PCS/UMTS). The antenna array is mainly composed of five lower-band elements, ten upper-band elements, some U-shaped metal baffles, and a metal reflector with specific shape. In order to reduce the overall size of the antenna array, lower-band element is designed as octagon aperture shape that upper-band elements can be embedded in it. Two kinds of radiation elements (five for each kind of element) are applied in the antenna array as upper-band elements to achieve better radiation performance. The proposed antenna array achieves electrical downtilt (0°–14° and 0°–10° at lower frequency band and upper frequency band, respectively) by adjusting input amplitude and phase of each array element. Measured results demonstrate that the antenna array has good broadside radiation characteristics, including low voltage standing wave ratio (VSWR $<$ 1.5), high port-to-port isolation ($>$28 dB), low backlobe level ($>$25 dB), high cross-polarization discrimination ($>$20 dB), and stable radiation pattern with horizontal half-power beamwidth (HPBW) 65° $\pm$ 5° at both frequency bands and all electrical downtilt angles. The peak gains of 15.1 and 17.3 dBi are obtained at lower and upper bands respectively. Owing to these advantages, the antenna array is suitable for existing 2G/3G applications in modern mobile communication systems.

INDEX TERMS Base station antenna array, dual-broadband, dual-polarized, electrical downtilt.

I. INTRODUCTION

With rapid development of various generations of mobile communication systems, antennas with wide frequency bandwidth are preferred in modern base station antenna applications because they can support multi-network communication systems simultaneously and reduce the overall number of antennas on cellular base stations. Nowadays, there is an increasing demand for base station antennas capable of operating at both 2G and 3G frequency bands, including European Digital Dividend (0.79-0.862 GHz), CDMA800 (0.82-0.88 GHz), GSM900 (0.88-0.96 GHz), DCS (1.71-1.88 GHz), PCS (1.85-1.99 GHz) and UMTS (1.92-2.17 GHz) bands.

In the last decades, base station antennas have attracted much attention and various kinds of base station antennas with different structures were investigated and proposed, including patch antennas [1], [2], cross-dipole antennas [3]–[5], magneto-electric dipole antennas [6], etc. Furthermore, polarization diversity technique (especially slant ±45° polarization) is popular in base station antenna design due to its ability in increasing system capacity and combating the issue of multipath fading [7]. A dual-polarized double E-shape patch antenna with high isolation and compact size was proposed in [1], but the bandwidth of this antenna is not wide enough to cover 2G and 3G services. In [2], a dual-band and dual-polarized stacked patch antenna with aperture coupling feed was proposed. It had good radiation characteristics at both lower and upper bands, but the complex structure limited its applications. A slant ±45° dual-polarized cross dipole with parasitical crossed-strip and a novel magneto-electric dipole were presented in [3] and [6] respectively. Although they had wider impedance bandwidth than the aforementioned antennas, VSWRs of the two antennas were larger than 1.9 which did not meet the industry

standard (VSWR < 1.5) of modern base station antenna design.

It is common to arrange antenna elements as antenna array to achieve higher gain and better directivity [10]–[12]. One of the most important part in designing a multi-band antenna array is to reduce mutual coupling between elements operating at different frequency bands. There are two typical approaches to solve this issue. One approach was to arrange antenna elements side by side [8] to increase the distance between subarrays, while the overall size of the antenna array is increased greatly. The other approach was to employ decoupling network [9] to improve port-to-port isolation. In recent years, a new arrangement scheme for antenna array called embedded scheme was illustrated in [13]. Lower-band elements were designed as hollow bowl structure so that upper-band elements can be embedded in ''bowl''. A large reduction in the size of antenna array is realized by using embedded scheme.

In densely populated urban areas, base station antennas are needed to dynamically adjust downtilt angles to improve spatial isolation and avoid mutual interference with adjacent antennas. By manipulating input magnitude and phase of each array element, main lobe coverage area of an antenna array can be steered, which is called electrical downtilt. Compared with traditional mechanical downtilt, electrical downtilt has lots of advantages, including less loss, easier to adjust and less influence on radiation patterns [14]. However, many literatures only focused on the performance of base station antennas radiating at a fixed angle [13], [15], [16] while the performance of an antenna array at downtilt angles received few attention.

For these reasons, a compact dual-broadband dual-polarized electrical downtilt base station antenna array is presented in this paper. The proposed antenna array has impedance bandwidth of 19.4% in the low frequency band and 23.7% in the high frequency band with VSWR < 1.5. High measured port-to-port isolation larger than 28 dB and stable radiation patterns with horizontal half-power beamwidth 65°±5° are achieved at both bands and all electrical downtilt angles. Five lower-band elements and ten upper-band elements with good electrical and mechanical characteristics are applied in the antenna array to achieve high gain. The antenna array adopts embedded scheme to reduce array size. Additionally, the whole structure of the antenna array is stable and easy to fabricate, which is suitable for existing 2G/3G mobile communication systems.

II. ANTENNA RADIATION ELEMENT

A. LOWER-BAND RADIATION ELEMENT

A novel wideband dual-polarized antenna element covering 0.79-0.96 GHz frequency band was illustrated in [17] and applied in the proposed antenna array as lower-band radiation element. The radiation element is designed as octagon aperture shape to realize embedded scheme and reduce the mutual coupling with internal upper-band radiation element.

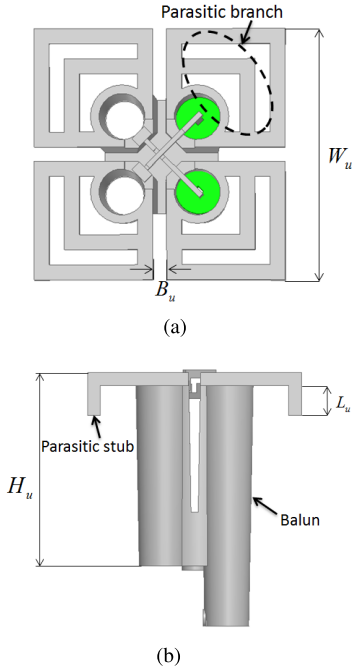

FIGURE 1. The internal upper-band radiation element. (a) top view; (b) side view.

It consists of two pairs of symmetrical dipoles, four couples of baluns, a base bottom and two kinds of plastic fasteners (four for each kind of fastener). Among the four dipoles, each pair of opposite dipoles excite one polarization and the two polarizations are orthogonal. Mutual coupling is generated between adjacent dipoles through bent radiation arms, which helps increase bandwidth and improves radiation performance.

B. UPPER-BAND RADIATION ELEMENT

Two kinds of broadband dual-polarized antenna elements are applied in the proposed antenna array as upper-band elements. One is placed between two adjacent lower-band elements and the other one is embedded in lower-band element. The external upper-band element was proposed in [19]. It consists of two crossed-dipoles, two couple of baluns and a pair of inverted L-shaped feeding strips [18]. Simulated and measured results showed that the radiation element has wide impedance bandwidth and relatively stable radiation pattern over the working frequency band.

The configuration of the internal upper-band radiation element is shown in Fig. 1. This element is similar to the external element and contains two crossed-dipoles, two couple of baluns and a pair of inverted L-shaped feeding strips. The two couples of baluns are designed to provide balanced transmission and support the whole radiation element. Two major differences with the external upper-band element can be concluded as follows: 1) In each square-loop radiation arm, a pair of parasitic metal branches are replaced by a L-shaped metal branch, which can also increase the current path; 2) the internal element is higher than the external one,

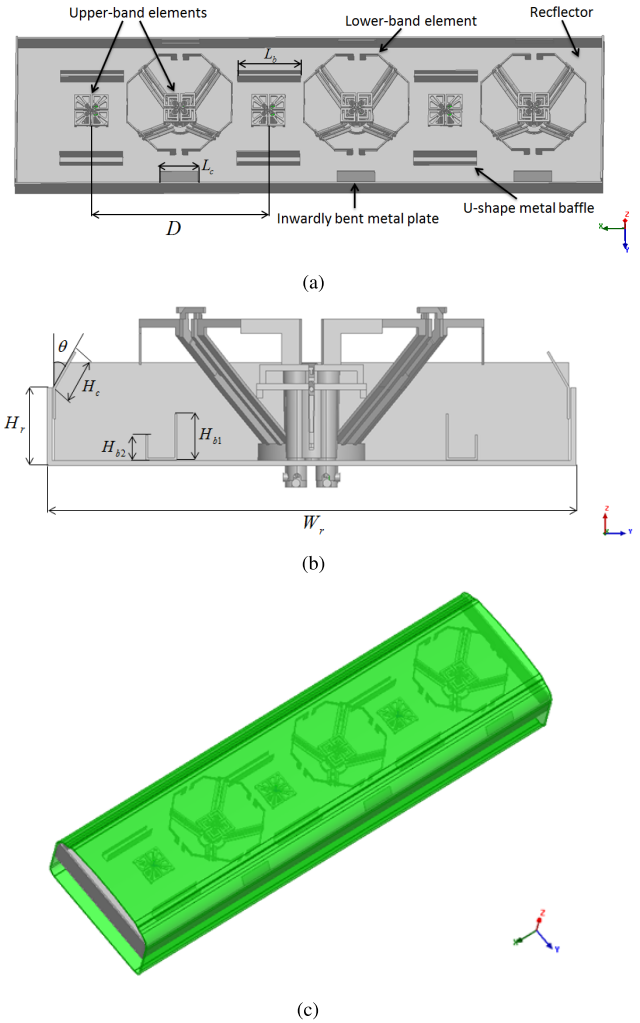

FIGURE 2. Simplified antenna array simulation model. (a) top view; (b) sectional view; (c) full view.

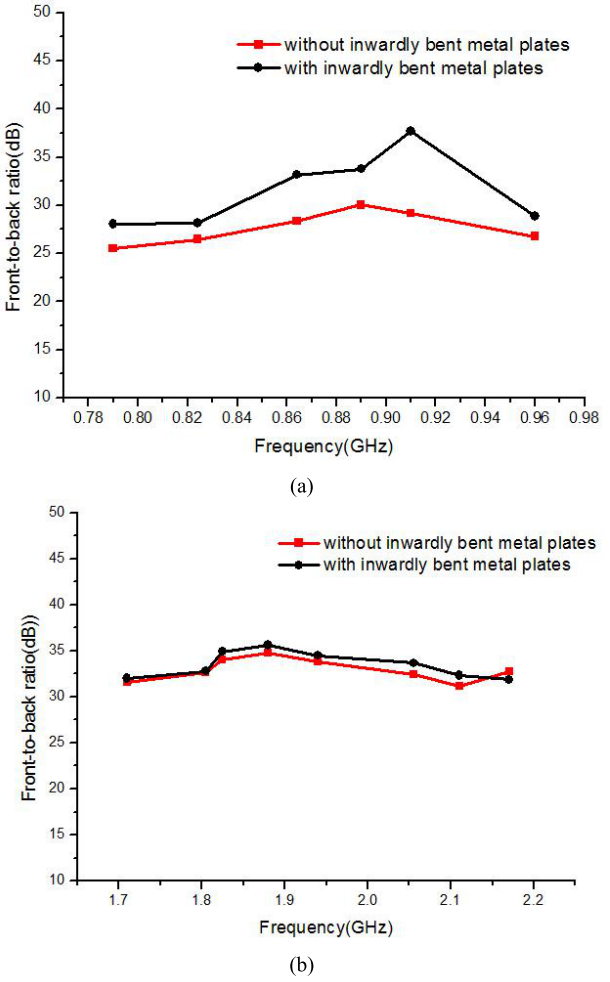

FIGURE 3. Simulated front-to-back ratio with and without inwardly bent metal plates. (a) lower frequency band; (b) upper frequency band.

so the height of balun is larger than quarter-wavelength. The L-shaped metal branch can be treated as a parallel branch of radiation arm, which acts as an impedance transformer to the radiation element and has a impact on the impedance bandwidth of the radiation element. In embedded scheme, internal upper-band element with greater height can decrease the shielding effect from lower-band element. Therefore, with this particular design, the proposed internal element facilitates the radiation performance improvement, which is shown in section III. Detailed parameters of the internal upper-band element shown in Fig. 1 are listed in Table 1.

The two upper-band elements are fabricated by integrated metal casting technology and have the advantages of stable structure, light weight, good consistency and easy to assemble.

III. ANTENNA ARRAY DESIGN

In order to achieve higher gain and better directivity, five lower-band radiation elements and ten upper-band radiation

TABLE 1. Specific parameters of radiation elements and antenna array.

Parameter	Value	Parameter	Value	Parameter	Value
B_u	2.8 mm	W_u	50 mm	H_u	45 mm
L_u	7 mm	L_b	100 mm	L_c	60 mm
D	140 mm	H_r	37.5 mm	H_c	20 mm
H_{b1}	22 mm	H_{b2}	12 mm	W_r	255 mm
θ	30°				

elements are applied in the proposed antenna array. The number of array elements have great impact on antenna gain and vertical plane (E-plane) radiation patterns, while have less influence on horizontal plane (H-plane) radiation patterns. For ease of simulation, a simplified antenna array containing three lower-band elements and six upper-band elements is done. The configuration of the simulation model and corresponding coordinate system are shown in Fig. 2. It mainly consists of a metal reflector with specific shape, three lower-band radiation elements, six upper-band radiation elements and some U-shape metal baffles which are located

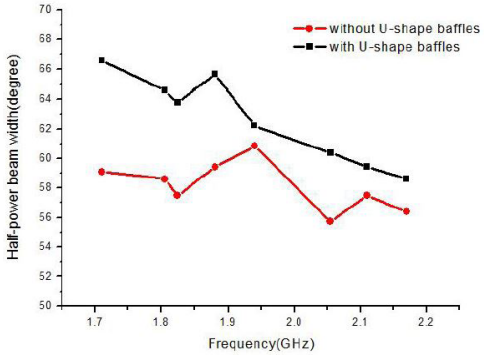

FIGURE 4. Simulated horizontal HPBW with and without U-shape metal baffles.

on both sides of external upper-band elements along vertical direction. Furthermore, a FRP (fiber reinforced plastic) radome (relative dielectric constant of 3.78) is included in simulation model to provide more accurate simulation as shown in Fig. 2(c).

A. DESIGN OF THE REFLECTOR AND U-SHAPED METAL BAFFLES

Since the horizontal plane radiation pattern is affected by the reflector, a metal reflector with specific shape and some U-shaped metal baffles are designed to pilot the antenna radiating to desired direction. The reflector and metal baffles are all made of aluminum, so they have good conductivity, relatively light weight and low cost. Thickness of the reflector and metal baffles are 2.5 mm and 1 mm, respectively. Inwardly bent metal plates are added to the vertical part of the reflector to further improve front-to-back ratio of the antenna array. Simulated front-to-back ratio (FBR) of the simplified antenna array with and without inwardly bent metal plates are shown in Fig. 3. Simulated results demonstrate that inwardly bent metal plates are beneficial to improve lower-band FBR while have little impact on upper-band FBR. The minimum lower-band FBR is increased from 25.5 dB to 28 dB while the FBR at upper-band is larger than 30 dB after adding the inwardly bent metal plates.

In densely populated urban areas, base station antennas with horizontal half-power beamwidth (HPBW) around 65° can achieve optimal coverage and reduce mutual interference with adjacent antennas. Fig. 4 shows that the horizontal HPBW of the antenna array without metal baffles ranges from 55.7° to 60.8° at upper frequency band, which will generate coverage blind area in practical applications. In order to broaden the upper-band horizontal HPBW, U-shaped metal baffles are placed at both sides of external upper-band elements along x-axis. After adding U-shaped metal baffles, the upper-band horizontal HPBW ranges from 59° to 66.5°, which meets the general standard of practical applications. Specific parameters of the reflector and the U-shaped metal baffles are optimized and also tabulated in Table 1.

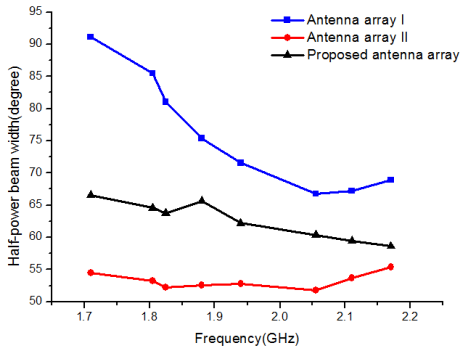

(a)

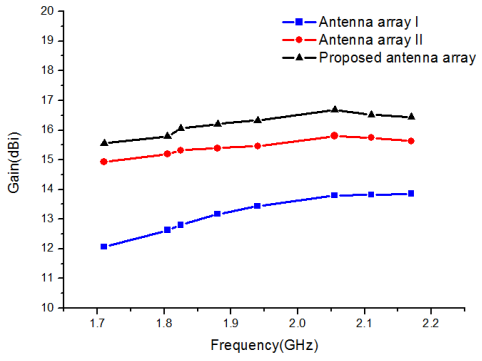

(b)

FIGURE 5. Simulated horizontal HPBW and gain at upper frequency band. (a) horizontal HPBW; (b) antenna array gain.

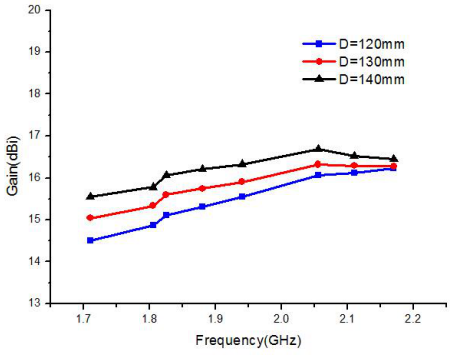

FIGURE 6. Antenna array gain at upper frequency band.

B. ANTENNA USING DIFFERENT UPPER-BAND RADIATION ELEMENTS

In order to demonstrate the advantages of the proposed array, antenna arrays using single type upper-band element are compared with the proposed antenna array. Internal upper-band elements are replaced by external upper-band element in antenna array I, and vice versa in antenna array II. The two antenna arrays have the same radiation boundaries and excitations with the proposed antenna array. Fig. 5(a) and Fig. 5(b) present horizontal HPBW and antenna array gain at upper frequency band of these three antenna arrays respectively.

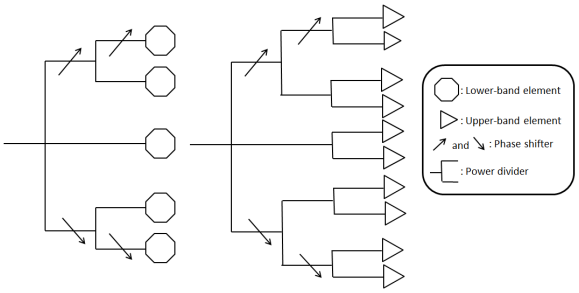

FIGURE 7. Feed networks configuration, left: the lower-band feed network; right: the upper-band feed network.

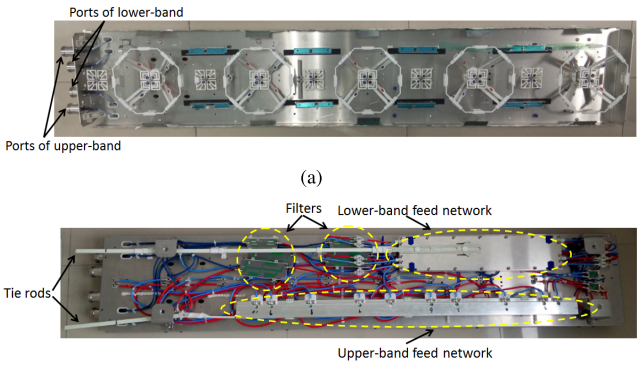

FIGURE 8. Prototype of the proposed antenna array. (a) front view; (b) back view.

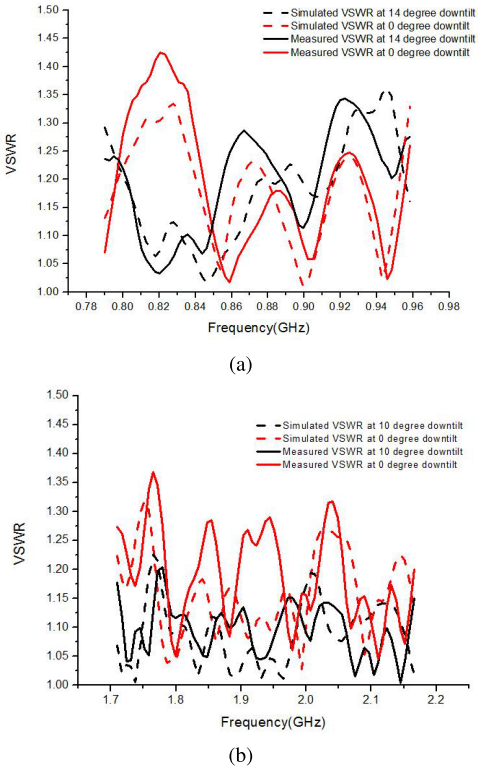

FIGURE 9. Simulated and measured VSWR of the antenna array. (a) lower-band VSWR; (b) upper-band VSWR.

The horizontal HPBW of antenna array I ranges from 67° to 91°, which is far larger than 65°. Since lower-band element is significantly higher than upper-band element, it would suppress radiation of internal upper-band element and decrease the antenna gain. Moreover, poor directivity also leads to low antenna gain, so the gain of antenna array I is lower than other antenna arrays.

In order to solve the shielding effect in embedded scheme, a relatively high radiation element is specially designed. The gain of antenna array II is improved compared to antenna array I, while the horizontal HPBW ranges from 51.7° to 55°, which is relatively narrower than optimum horizontal HPBW. For these reasons, two different kinds of upper-band elements are located at different positions to form the proposed antenna array. Simulated results demonstrate that the proposed antenna array has higher gain and better directivity than the other two antenna arrays.

C. SPATIAL DISTANCE BETWEEN ADJACENT ELEMENTS

It is known that the vertical directivity of a broadside antenna array are related to the number of radiation elements, spatial distance between two adjacent elements and corresponding working frequency band [20], which is defined by:

$$D_0 = 2N\left(\frac{D}{\lambda}\right) \tag{1}$$

where N is the number of radiation elements, D is the spatial distance between two adjacent elements and λ is the wavelength corresponding to the operating frequency. Additionally, the gain of an antenna array increases with the increase of directivity. In broadside antenna array design, the separation between two adjacent elements are less than one wavelength so that there are no principal maxima in other directions, which are referred to as grating lobes [20].

In the proposed antenna array, the upper frequency band is in the range from 1.71 GHz to 2.17 GHz, so the corresponding wavelength range is from 140 mm to 175 mm. Therefore, the separation between two adjacent elements is set to 140 mm to obtain the highest gains and avoid grating lobes. Simulated gains at different spatial distances are presented in Fig. 6. It illustrates that with the increase of spatial distance, the maximum gain of the antenna array also increases. When $D = 140$ mm, the simulated peak gain is 16.7 dBi at 2.05 GHz. In embedded scheme, the separation between lower-band elements is twice as large as that of upper-band elements, which is also less than one wavelength at lower band.

D. ELECTRICAL DOWNTILT

Considering a N-element liner antenna array with equal separation D, the array factor is defined in [20]:

$$AF = \sum_{n=1}^{N} I_n e^{j(n-1)(kD\cos\theta+\beta_n)} \tag{2}$$

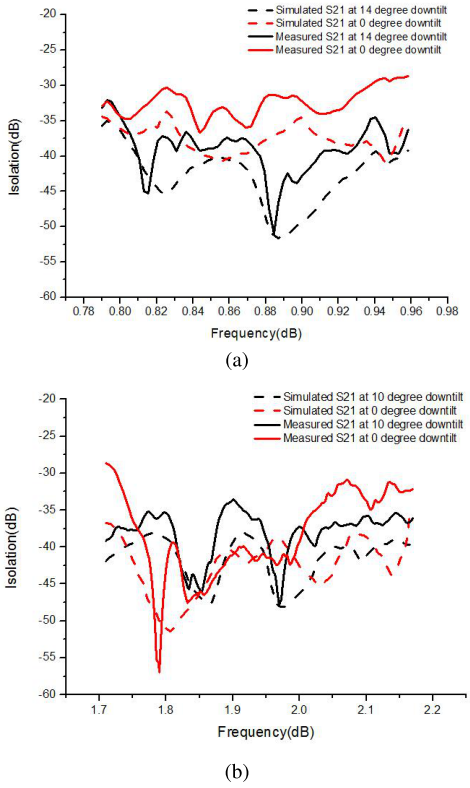

FIGURE 10. Simulated and measured isolation of the antenna array. (a) lower-band S_{21}; (b) upper-band S_{21}.

where I_n and β_n are input amplitude and phase of the n'th element respectively, θ is the angle between field spot and the array axis. By adjusting magnitude and phase of each array element, the proposed antenna array realizes electrical downtilt (0°-14° and 0°-10° for lower frequency band and upper frequency band, respectively). Two separated feed networks are designed for five lower-band radiation elements and ten upper-band radiation elements, respectively. They mainly consist of an unequal power divider, a low loss transmission device and several coaxial cables. When the tie rod is pulled, length differences between the transmission path of array elements are generated, which results in phase change of the corresponding array elements. In addition, the lengths of the coaxial cables can also be tuned to adjust the phase for each element. The two feed networks are shown in Fig. 7. The phase of each array element decreases along the positive x-axis while the phase of the middle element is set to 0. In this manner, radiation direction of the antenna array shifts toward the positive x-axis.

IV. MEASURED RESULTS AND PERFORMANCE ANALYSIS

A prototype of the antenna array with five lower-band radiation elements and ten upper-band radiation elements is fabricated, which is shown in Fig. 8. The overall size of the radome is 1420 mm × 260 mm × 130 mm. The length of the presented array is smaller than that (1500 mm) of existing antenna array. Measured VSWR and port-to-port isolation are

TABLE 2. Specific results of measured H-plane radiation patterns.

Downtilt	Fre (GHz)	HPBW (°)	FBR ±30° (dB)	XPD 0° (dB)
0°	0.79	67.72	28.17	25.09
	0.89	66.85	33.78	22.40
	0.96	62.86	28.88	24.49
14°	0.79	69.54	26.62	27.93
	0.89	67.37	31.35	25.30
	0.96	64.40	25.69	20.05
0°	1.71	65.36	29.67	29.09
	1.92	65.59	34.74	21.44
	2.17	60.03	34.33	24.89
10°	1.71	62.34	29.81	22.72
	1.92	63.57	30.36	22.44
	2.17	60.60	30.14	24.19

obtained by vector network analyzer in an anechoic chamber while radiation patterns of the antenna array are measured by far-field test system. Two short linear-shape isolation baffles are appended beside the third and five upper-band elements and a long arc-shape isolation baffle is placed beside the first lower-band element to further improve upper-band and lower-band port-to-port isolations respectively. Moreover, filters are utilized in the antenna array to reduce mutual coupling between subarrays.

Simulated and measured VSWRs versus frequency at different downtilt angles are shown in Fig. 9. Considering the symmetry of the slant ±45° polarization, only one port is presented. Simulated and measured port-to-port isolations of the antenna array are shown in Fig. 10. The differences between the measurement results and simulation results are caused by the fabrication errors. As shown in Fig. 9, the simulated and measured VSWR of the antenna array are less than 1.45 at both working frequency bands. At lower frequency band, VSWR is less than 1.45 when the downtilt angle is 0°. With the downtilt angle shifting to 14°, VSWR decreases slightly and the maximum VSWR is less than 1.44. At upper frequency band, measured VSWR at 10° downtilt is less than 1.2. A large variation is observed when the downtilt angle is 10°, and the maximum VSWR increases to 1.37. It is thus concluded that VSWR of the antenna array becomes better with the increase of downtilt angle, especially at upper frequency band. Regarding the lower-band isolation results, simulated and measured S_{21} at 0° and 14° are less than −30 dB, which means a low mutual coupling is achieved between lower-band ports. At upper frequency band, the maximum value of measured S_{21} is −28.6 dB, which also meets the design requirements. There is no big difference between the maximum of the S_{21} when antenna array is directed to different downtilt angles.

Measured horizontal plane radiation patterns of the antenna array (co-polarization along +45° direction and cross-polarization along −45° direction) at 0.79 GHz,

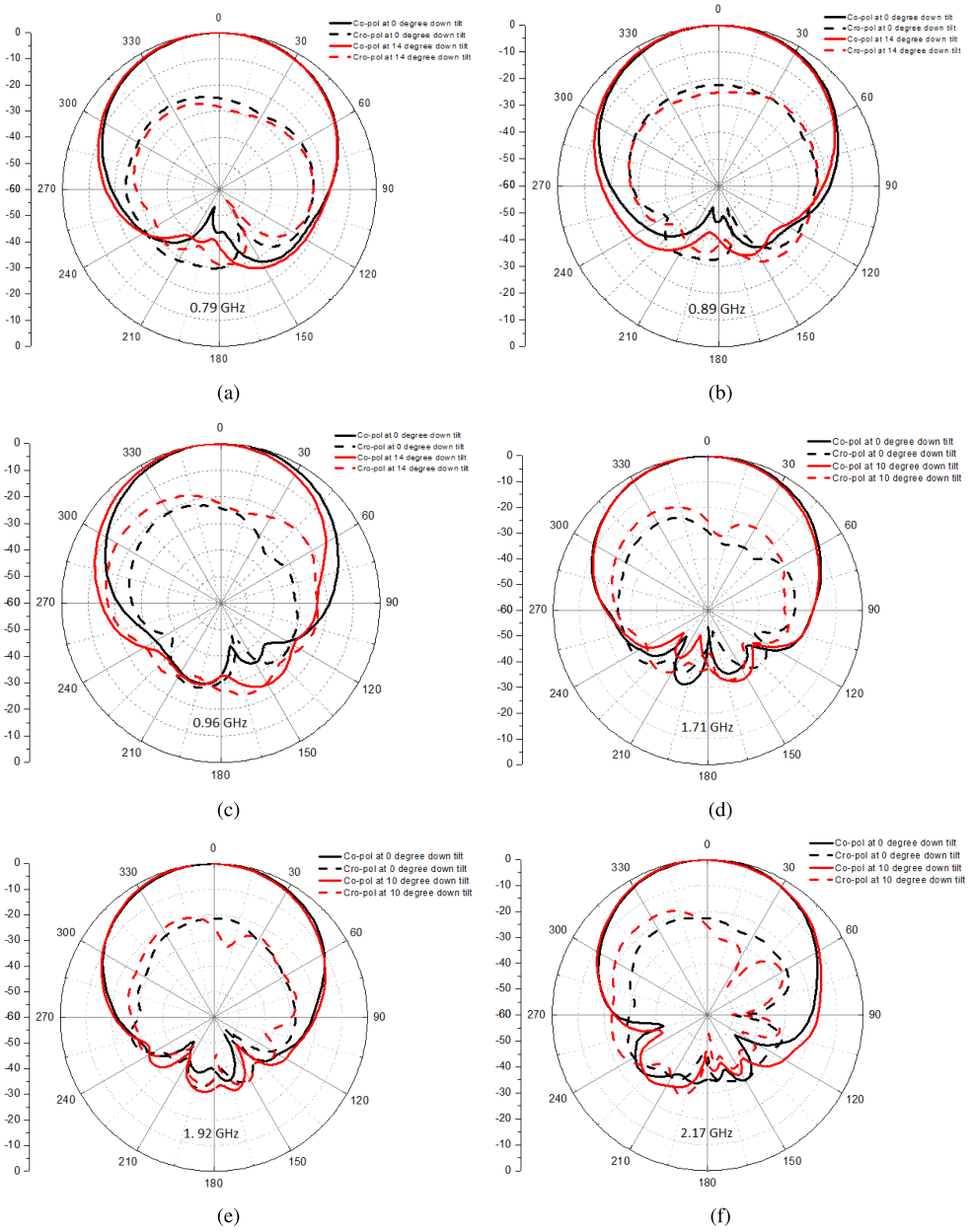

FIGURE 11. Measured H-plane radiation patterns of the proposed antenna array. (a) 0.79 GHz; (b) 0.89 GHz; (c) 0.96 GHz; (d) 1.71 GHz; (e) 1.92 GHz; (f) 2.17 GHz.

0.89 GHz, 0.96 GHz, 1.71 GHz, 1.92 GHz and 2.17 GHz are shown in Fig. 11. Due to the symmetry, radiation patterns for another polarization mode are omitted. As shown in the figure, the radiation patterns of the co-polarization are stable across the overall working band, and meanwhile, the radiation patterns of the cross-polarization get better as frequency increases in both frequency bands. Additionally, the radiation patterns distort mildly when the antenna array directs at 14° and 10° downtilt angles. As a result, stable H-plane radiation patterns with half-power beamwidth 65°±5° at both working bands are obtained. Moreover, low backlobe level (FBR > 25 dB), high cross-polarization discrimination (XPD> 20 dB) are achieved at the whole operating band and all downtilt angles. Specific values of HPBW, FBR and XPD in H-plane are shown in Table 2.

In general, suppressing the first upper sidelobe level below the main beam of vertical radiation patterns is required in base station antenna array design. Fig. 12 shows the measured realized gain radiation patterns of E-plane. It is obvious that the upper sidelobe level (theta > 0°) in both frequency bands and all downtilt angles are below −15 dB, which meets the design requirements. The E-plane radiation patterns are sightly worse when the antenna array directs at large downtilt angles. Especially at upper frequency band, sidelobe levels

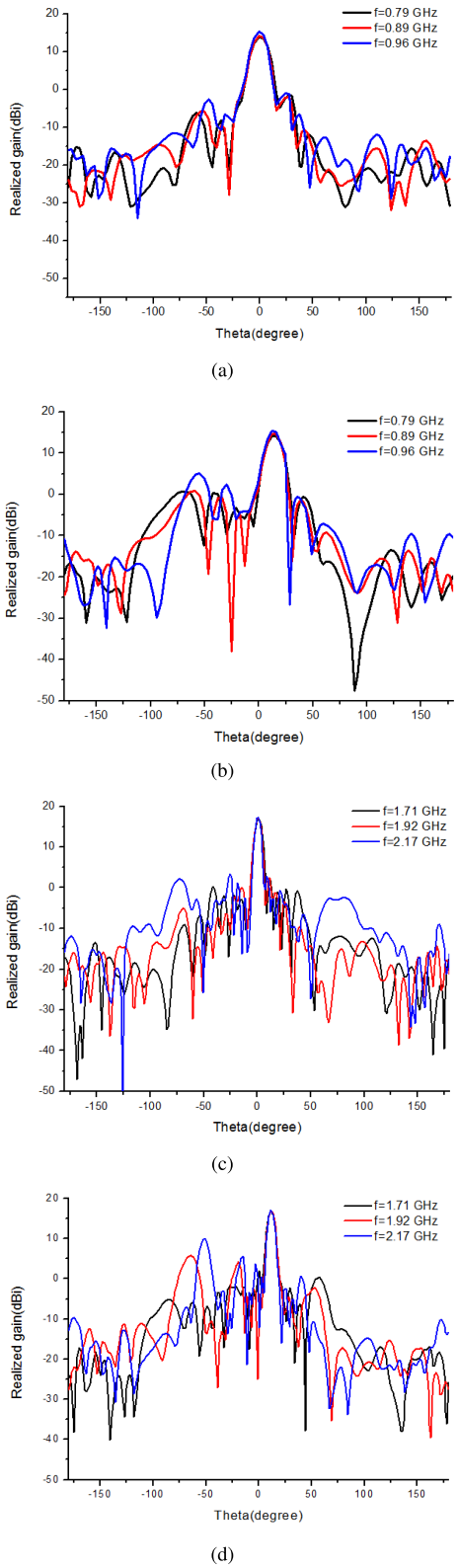

FIGURE 12. Measured E-plane radiation patterns of the proposed antenna array. (a) 0° downtilt at lower band; (b) 14° downtilt at lower band; (c) 0° downtilt at upper band; (d) 10° downtilt at upper band.

become higher (theta $<$ 0°) when the antenna array points at 10° downtilt angle, which leads to gain loss. HPBW in E-plane is around 14° at lower frequency band and 6° at upper frequency band. The realized peak gain of the proposed antenna array is 15.1 dBi at lower frequency band and 17.3 dBi at upper frequency band, respectively (both at 0° downtilt).

V. CONCLUSION

A dual-broadband dual-polarized base station antenna array operating at 0.79-0.96 GHz and 1.71-2.17 GHz is presented in this paper. By manipulating input amplitude and phase of each array element, 0°-14° and 0°-10° electrical down tilt are achieved at lower and upper frequency band respectively. Simulated and measured results demonstrate that the antenna array has good radiation characteristics at both working bands and all downtilt angles, including low VSWR ($<$ 1.5), high port-to-port isolation (S_{21} $<$ -28 dB) and stable radiation patterns with horizontal half-power beamwidth 65°$\pm$5°. The realized peak gains of 15.1 dBi and 17.3 dBi are obtained at lower and upper frequency band respectively. In addition, the antenna array has good mechanical characteristics, including compact structure, low profile, good stability and easy to fabricate. These advantages make the antenna array a good candidate for 2G and 3G services in modern mobile communication system.

ACKNOWLEDGEMENT

The authors appreciate MOBI Antennas Technologies (Shenzhen) Co., Ltd. for their assistance in fabricating the antenna.

REFERENCES

[1] Y. Gou, S. Yang, Q. Zhu, and Z. Nie, "A compact dual-polarized double e-shaped patch antenna with high isolation," *IEEE Trans. Antennas Propag.*, vol. 61, no. 8, pp. 4349–4353, Aug. 2013.

[2] M. Kaboli, M. S. Abrishamian, S. A. Mirtaheri, and S. M. Aboutorab, "High-Isolation XX-Polar Antenna," *IEEE Trans. Antennas Propag.*, vol. 60, no. 9, pp. 4046–4055, Sep. 2012.

[3] S. Zuo, Q. Liu, and Z. Zhang, "Wideband dual-polarized crossed-dipole antenna with parasitical crossed-strip for base station applications," *Progr. Electromagn. Res. C*, vol. 48, pp. 159–166, Jan. 2014.

[4] Y. Liu, H. Yi, F. W. Wang, and S. X. Gong, "A novel miniaturized broadband dual-polarized dipole antenna for base station," *IEEE Antennas Wireless Propag. Lett.*, vol. 12, no. 4, pp. 1335–1338, Oct. 2013.

[5] G. Cui, S.-G. Zhou, G. Zhao, and S.-X. Gong, "A compact dual-band dual-polarized antenna for base station application," *Prog. Electromagn. Res. C*, vol. 64, pp. 61–70, Jan. 2016.

[6] S. Chen and K. M. Luk, "High performance dual-band dual-polarized magneto-electric dipole base station antenna," in *Proc. Asia–Pacific Microw. Conf. (APMC)*, Sendai, Japan, Nov. 2014, pp. 321–323.

[7] R. G. Vaughan, "Polarization diversity in mobile communications," *IEEE Trans. Veh. Technol.*, vol. 39, no. 3, pp. 177–186, Aug. 1990.

[8] N. Amiri, K. Forooraghi, and R. Dehbashi, "A compact dual-polarized aperture-coupled stacked patch antenna for GSM900 MHz," in *Proc. IEEE Asia–Pacific Symp. EMC*, Dec. 2006, p. 3.

[9] L. Zhao and K. L. Wu, "A dual-band coupled resonator decoupling network for two coupled antennas," *IEEE Trans. Antennas Propag.*, vol. 63, no. 7, pp. 2843–2850, Jul. 2015.

[10] Y. Zhang, X. Y. Zhang, L. H. Ye, and Y. M. Pan, "Dual-band base station array using filtering antenna elements for mutual coupling suppression," *IEEE Trans. Antennas Propag.*, vol. 64, no. 8, pp. 3423–3430, Jun. 2016.

[11] K. Moradi and S. Nikmehr, "A dual-band dual-polarized microstrip array antenna for base stations," *Prog. Electromagn. Res.*, vol. 123, no. 1, pp. 527–541, 2012.

[12] H. J. Xu, X. W. Zhu, and Z. Q. Kuai, "Broadband dual-polarized planar antenna and array for mobile communication base station," in *Proc. Asia–Pacific Microw. Conf.*, Dec. 2015, pp. 1–3.
[13] Y. He, Z. Pan, X. Cheng, and Y. He, "A novel dual-band, dual-polarized, miniaturized and low-profile base station antenna," *IEEE Trans. Antennas Propag.*, vol. 63, no. 12, pp. 5399–5408, Dec. 2015.
[14] F. Athley and M. N. Johansson, "Impact of electrical and mechanical antenna tilt on LTE downlink system performance," in *Proc. Veh. Technol. Conf.*, May 2010, pp. 1–5.
[15] Z. J. Z. Liu Liu Liu, Y. Zhang, and X. Y. Zhang, "A novel dual-band and high-gain antenna for 2G/3G base station," *Progr. Electromagn. Res. Lett.*, vol. 54, no. 3, pp. 1–6, Jan. 2015.
[16] X. Jiang, Z. Zhang, Z. Tian, Y. Li, and Z. Feng, "A low-cost dual-polarized array antenna etched on a single substrate," *IEEE Antennas Wireless Propag. Lett.*, vol. 12, pp. 265–268, 2013.
[17] Y. He and W. Tian, "A broadband dual-polarized base station antenna element for European Digital Dividend, CDMA800 and GSM900 applications," in *Proc. Int. Wireless Commu. and Mobile Computing Conf.*, Jun. 2017, pp. 659–663.
[18] Q. Liu and B. Liu, "Ultra wideband radiation element and its base station antenna for mobile communication," Chinese Patent CN 204 966 674U, Jan. 13, 2016.
[19] Y. He and Y. Yue, "A novel broadband dual-polarized dipole antenna element for 2G/3G/LTE base stations," in *Proc. IEEE Int. Conf. RFID Technol. Appl.*, Sep. 2016, pp. 102–106.
[20] C. A. Balanis, *Antenna Theory Analysis and Design*. Hoboken, NJ, USA: Wiley, 2005.

YEJUN HE (SM'09) received the Ph.D. degree in Information and Communication Engineering from Huazhong University of Science and Technology, Wuhan, China, in 2005. From 2005 to 2006, he was a Research Associate with the Department of Electronic and Information Engineering, The Hong Kong Polytechnic University, Hong Kong. From 2006 to 2007, he was a Research Associate with the Department of Electronic Engineering, Faculty of Engineering, The Chinese University of Hong Kong, Hong Kong. In 2012, he was a Visiting Professor with the Department of Electrical and Computer Engineering, University of Waterloo, Waterloo, ON, Canada. From 2013 to 2015, he was an Advanced Visiting Scholar (Visiting Professor) with the School of Electrical and Computer Engineering, Georgia Institute of Technology, Atlanta, GA, USA. Since 2011, he has been a Full Professor with the College of Information Engineering, Shenzhen University, Shenzhen, China, where he is currently the Director of the Shenzhen Key Laboratory of Antennas and Propagation, and the Director of the Guangdong Engineering Research Center of Base Station Antennas and Propagation. He has authored or coauthored over 100 research papers, books (chapters) and holds about 20 patents. His research interests include wireless mobile communications, antennas and RF. He has served as a Technical Program Committee Member or a Session Chair for various conferences, including the IEEE Global Telecommunications Conference, the IEEE International Conference on Communications, the IEEE Wireless Communication Networking Conference, and the IEEE Vehicular Technology Conference. He has also served as a Reviewer for various journals, such as the IEEE TRANSACTIONS ON VEHICULAR TECHNOLOGY, the IEEE TRANSACTIONS ON COMMUNICATIONS, the IEEE TRANSACTIONS ON WIRELESS COMMUNICATIONS, the IEEE TRANSACTIONS ON INDUSTRIAL ELECTRONICS, the IEEE WIRELESS COMMUNICATIONS, the IEEE COMMUNICATIONS LETTERS, the IEEE JOURNAL ON SELECTED AREAS IN COMMUNICATIONS, the *International Journal of Communication Systems*, the *Wireless Communications and Mobile Computing*, and the *Wireless Personal Communications*. He is currently serving as an Associate Editor of the IEEE ACCESS and the *Security and Communication Networks*. He is a Fellow of IET.

WEI TIAN is currently pursuing the master's degree with Shenzhen University, Shenzhen, China. His research interests include base station antennas and RF.

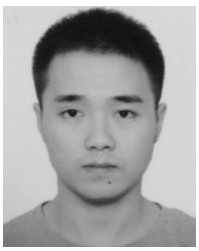

LONG ZHANG received the B.S. and M.S. degrees in Electrical Engineering from the Huazhong University of Science and Technology, Wuhan, China, in 2009 and 2012, respectively, and the Ph.D. degree from the University of Kent, Canterbury, U.K., in 2017. He is currently with the College of Information Engineering, Shenzhen University, China. His research interests include antennas and RF. He served as a Reviewer for several technique journals, including the IEEE TRANSACTIONS ON ANTENNAS AND PROPAGATION, the *IET Microwaves, Antennas & Propagation*, and the *Electronics Letters*.